Methods and objects of chemical analysis, 2024, Vol. 19, No. 4, 226–234

New Semi-IPN hydrogels for Removal of High Concentrated Congo Red Dye from Aqueous Solutions

Noor D. Jaffer*†, Safa M. Hameed†, and Athir M. Haddad‡

†Chemistry Department, Faculty of Education for Women, University of Kufa, Albuhadari St., P.O. Box 21, Kufa, Najaf Governorate, 54003, Iraq;
‡ Chemistry Department, College of Science, University of Basrah, Qarmat Ali Campus, Basrah, Iraq;
*e-mail: noord.almossawy@uokufa.edu.iq

Received: July 24, 2024; Accepted: October 17, 2024
DOI: 10.17721/moca.2024.226-234

Six semi-IPN hydrogels (N1–N6) were synthesized by redox polymerization with different molar ratios of 2-(dimethylamino)ethyl methacrylate (DMAEMA) and sodium alginate. Methylene-bisacrylamide acted as a crosslinker for DMAEMA, and calcium chloride was used as a crosslinking agent for sodium alginate. The synthesized semi-IPN hydrogels are characterized by swelling ratio, scanning electron microscopy (SEM), BET, thermal gravimetric analysis (TGA), and differential scanning calor. The adsorption capacities of the prepared hydrogel polymers for the removal of Congo red dye from their aqueous solutions were studied at an initial concentration of 700 ppm. N3 and N4 hydrogels exhibited the highest adsorption capacities. The optimum pH and temperature were found to be 7 and 65 °C, respectively, resulting in adsorption capacities of 1365 mg/g and 1328 mg/g, with adsorption percentages of 97.53% and 94.857% for N3 and N4, respectively. The adsorption behavior of both hydrogel adsorbents followed Langmuir's model. It exhibited pseudo-second-order kinetics during the adsorption of CR dye, referring to the adsorption of CR on N3 and N4 adsorbents as chemisorption. The thermodynamic parameters have been calculated, and they refer to endothermic, randomness, and spontaneous adsorption. Desorption experiments were also performed, and NaOH was identified as the most effective eluent for CR dye recovery.

Keywords: hydrogel, Semi-IPN, DEMAEMA, sodium alginate, adsorption, congo red

Introduction

Water pollution is a significant global issue due to the crucial role of water in our daily lives [1]. Synthetic dyes, which are stable and highly soluble in water, are common pollutants in industrial wastewater [2,3]. The textile industry is one of the most common industrial activities that generate toxic colored wastewater [4] besides dyeing and printing, paper and pulp, cosmetics, food, pharmaceuticals, oil, and photographic colors [5]. About 7 x 10^7 tons of synthetic dyes are produced annually worldwide, with approximately 10% being discharged into water bodies [6]. Organic dyes were studied closely due to their danger and toxicity; they can cause cancer even at low concentrations [7]. These can cause serious health problems, including damage to the liver, kidney, and nervous system, as well as various cancers [8].

Azo dyes are a vital colorant that constitutes two-thirds of all synthetic dyes and is responsible for more than 50% of the annual global manufacturing of dyes. They are toxic, mutagenic, and carcinogenic agents [9]. Congo red (CR) is an anionic dye that causes allergic and metabolizes to a human carcinogen called benzidine [10]. It promotes mutagenic and carcinogenic activities [11]. Accumulation of Congo red dye leads to blood clotting, skin and eye irritation, digestive system disorders, and breathing difficulties. It may also cause drowsiness and allergic reactions [12].

Adsorption is an efficient, easy-to-use, and cost-effective technique for water purification [13] compared to other methods for water treatment, such as precipitation, coagulation, degradation, oxidation, reverse osmosis, and others [14]. Adsorption refers to the process of molecules aggregating onto the surface of an adsorbent material [15]. This process involves physical or chemical bonding of molecules with active sites on the surface, forming one or more layers of molecules [16,17]. The adsorption process is influenced by various factors, such as temperature, ionic strength, acid function, nature of the adsorbent, effect of equilibrium time, surface area of the adsorbent, and concentration of the adsorbent [18,19]. Several adsorption isotherms describe the equilibrium state between the solution and the solid phase of the adsorbent surface. These isotherms, such as the Langmuir, French, and others, give a clue about the nature of adsorption and the thermodynamic functions of the process [20,21].

The use of interpenetrating polymer networks (IPNs) and semi-IPN hydrogels as adsorbents for toxic dyes has attracted considerable attention because of their high swelling and adsorption performance,

structural stability, and non-toxicity [22,23]. Hydrogels also represent stimuli-responsive materials and adsorb due to light, pH, temperature, ionic strength, and electric field [24]. PDMAEMA is among those polymeric materials that are very sensitive to changes both in pH and temperature, hence being widely used in various areas such as drug delivery systems, membranes, sensors, and antibacterial materials [25]. Sodium alginate is a natural linear polysaccharide that is highly safe, biodegradable, and biocompatible [26]. It is widely used in industry due to its stability, strength, flexibility, and ability to swell and retain water. Sodium alginate is a natural linear polysaccharide that is highly safe, biodegradable, and biocompatible. It is widely used in industry due to its stability, strength, flexibility, and ability to swell and retain water [27]. Various bacteria and brown algae synthesize Alginate. The extracted alginate is used in the food, pharmaceutical, and cosmetic industries. Sodium alginate is an anionic natural polymer used widely in drug delivery [28]. Six semi-IPNs from Poly(dimethylaminoethyl methacrylate) with Sodium alginate were prepared and used to remove Congo Red dye.

Experimental part

Materials and measurements

All chemicals were purchased from Merck and Sigma-Aldrich and used without any treatment; all solutions were prepared using deionized water. The structure and morphology of all prepared hydrogel Adsorbents were identified using The FESEM device with model TESCAN MIRA3 made in the Czech Republic, BORNA Science and Technology Institute, Tehran, Iran. The UV-visible spectra were recorded using a T80+ spectrophotometer at Kufa University, Iraq.

Preparation of semi-IPN hydrogels N1-N3

1 g of sodium alginate was dissolved in (10 mL) of deionized water. Gradually, 1g of N,N-Dimethylaminoethyl Methacrylate (DEMAEMA) was added with continuous stirring for 15 minutes using the magnetic stirrer to mix them thoroughly. 0.2 g of N,N-methylene bis acrylamide (BisAA) was added, and finally, 1 mL from the solution of sodium persulfate (10 % w/v) as an initiator with 0.2 mL from Tetra methyl ethylene diamine (TEMED) as the accelerator was added. Stirring is continued as the colour of the solution is observed to change to white with a significant increase in the density of the solution. The reaction was left for a few minutes until the crosslinking reaction was complete. It is placed in a drying oven at 50 °C for 24 hours until the semi-IPN (N1) dries completely. The same steps were repeated with different weight ratios from DEMAEMA to prepare the semi-IPN hydrogels N2 and N3 [29]. Table S1 shows the composition of the prepared semi-IPN hydrogels.

Preparation of copolymer hydrogels N4-N6

N4 semi-IPN was prepared by dissolving 1 g of DEMAEMA in 5 mL of deionized water with stirring, 0.3 g of sodium persulfate, the initiator, and 0.3 mL of the accelerator (TEMED) with continued stirring and heating at 50 °C within an hour, where turbidity of the solution is observed. A polymerization reaction begins to form the linear Poly DEMAEMA and is left in the oven for a whole night at 50 °C to complete the reaction. 1g of sodium alginate is dissolved in deionized water and added to the solution of Poly DEMAEMA. The mixture was stirred for 15 minutes to ensure the two linear polymers were mixed well. A 5% (wt./v) calcium chloride solution was used as a crosslinking agent for sodium alginate polymer. The Crosslinking reaction is done by dropping a solution of the polymer mixture in a beaker containing the solution of calcium chloride $CaCl_2$. These steps were repeated using 2 and 3 g of sodium alginate to prepare N5 and N6 [30,31]. Table 1 shows the composition of the prepared Semi-IPN hydrogels. The polymerization reaction is illustrated in Scheme 1.

Swelling ratio study

The swelling ratio of all the manufactured hydrogels was determined by measuring the weight of each hydrogel in its dried state (xerogel) and then immersing it in 50 mL of deionized water. The weight of the hydrogel was measured at various time intervals after the removal of surface water until it reached a state of equilibrium. The swelling ratio (Q) was determined by applying the equation [32].

$$Q\% = ((Ws - Wd) / Wd) * 100\%, \quad (1)$$

where Ws represents the weight of the hydrogel in its swollen state at the measured time interval and Wd represents the weight of the hydrogel in its dried state.

Preparation of aqueous Congo Red solution

Congo red dye, an ionic diazo dye with M.wt of 696.7, a stock solution of the dye with a concentration of (1,000 mg/L) was prepared for use in batch adsorption experiments, and then dilution was used to prepare the remaining required concentrations with deionized water. CR dye solutions were measured at λmax 483 nm using a Sentry 20 UV-visible spectrophotometer model T180.1. In a 1 cm length quartz cell [33].

Batch Adsorption Experiments

Adsorption experiments were conducted using the batch method to assess the factors influencing the adsorption process and determine the ideal conditions. The hydrogel adsorbents N1–N6 were mixed in 50 ml of CR dye solutions of different concentrations and used in amounts of 25 mg. The primary concentration of CR dye was selected, and the mixture was subjected to agitation in a thermostatic shaker at 225 RPM and 35 °C for 24 hours. Following the process of adsorption, the adsorbents were separated using filtration. The residual concentration of CR dye was then measured using a UV-visible spectrometer at 483 nm. Adsorption experiments were carried out at various agitation times (5, 15, 30, 60, 120, 150, 180, 240, 300) min and at different pH values including 3, 5, 7, 9, and 11. The amount of CR dye on the adsorbents

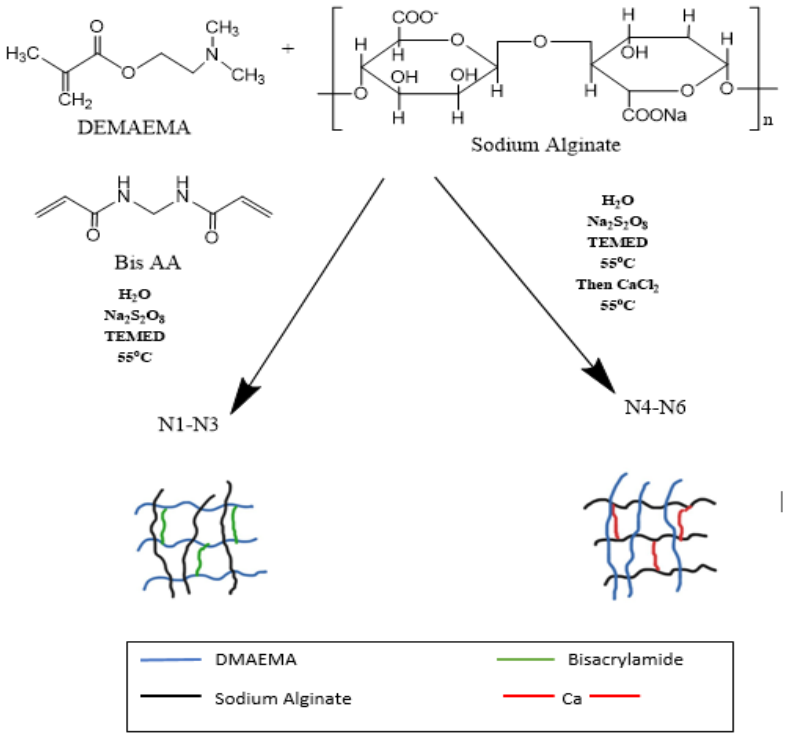

Scheme 1. The polymerization reaction of semi-IPN of (PDEMAEMA- sodium alginate) hydrogels.

was calculated by the equation below:

$$qe = ((C0 - Ce) / w) * V, \quad (2)$$

where C^0 and Ce (mg/L) are CR dye's initial and equilibrium concentrations, V (L) represents the volume of the CR solution, w (g) is the mass of the hydrogel, and qe (mg/ g) is the adsorption capacity [34,35].

Desorption study

The desorption of CR dye from the hydrogels was detected using repeated adsorption/desorption cycles. The dye-loaded adsorbent was immersed in 0.1 M of NaOH and HCl, which were used for the desorption experiments. The mixture was stirred at 65°C for 3 hours, and the desorbed dye was separated and filtered. The concentration of the dye was determined spectrophotometrically. The efficiency of CR dye desorption (S) is calculated using the following equation [36]:

$$S\% = (Cd * Vd / (qe * W)) * 100\%, \quad (3)$$

where C_d (mg /L) is the CR concentration after desorption, and Vd (L) is the eluent volume.

Adsorption Isotherms

Adsorption isotherms, such as the Langmuir and Freundlich models, are studied to explain the adsorption behavior and the relationship between the amount of adsorbed dye and the equilibrium concentration. The Langmuir and Freundlich linear forms are represented in equations 4 and 5, respectively (see Supplementary Material).

Kinetics studies

Kinetics data give helpful information about the adsorption process [37]. They can be assessed using various models, such as the pseudo-first and second order and Intra-particle diffusion models, tested in our study. The linear equations of these models are expressed by equations 6-8 (see Supplementary Material).

Adsorption Thermodynamics

Thermodynamic parameters of the adsorption process, including the change of the standard [enthalpy (ΔH°), entropy (ΔS°), and free energy (ΔG°)] can be calculated from the constant of thermodynamic equilibrium (K_L), which equals to Ca/Ce, Ca (mg/g) and Ce (g/L) represent the adsorbed and the remaining concentration of CR dye respectively. The thermodynamic parameters can be calculated by the equations 9-10 (see Supplementary Material).

Results and discussion

Semi-IPN hydrogels were synthesized using redox polymerization with a sodium persulfate initiator [40]. N,N-methylene bis acrylamide (BisAA), and calcium chloride were crosslinking agents for DEMAEMA and sodium alginate, respectively [41]. Accurately determining the swelling ratio of the prepared hydrogels is essential for assessing their effectiveness and potential uses [42]. Figure S1 show the swelling ratios of N1-N3 as a function of time. The swelling rate increases quickly at first, then steadily increases until it reaches equilibrium within two hours.

Figure S2 shows the swelling ratios of N4-N6, measured after 24 hours of immersion in water. The hydrogels N1-N3 undergo fragmentation upon

immersion in water, preventing the measurement of the swelling rate over time. The calculation was performed solely at the equilibrium state, precisely 24 hours later.

The swelling ratio of N1-N3 increases with increasing DEMAEMA content of the polymeric formulation, suggesting that DEMAEMA has a stronger impact on boosting the swelling ratio than sodium alginate. All the prepared hydrogels were determined to be super absorbent hydrogels [43].

Hydrogels' morphology, pore size, and porosity can be accurately determined using a scanning electron microscope (SEM) [44]. Figure 1 displays the scanning electron microscope (SEM) images of the swelling state of N1 and N6, which shows that the swollen structures contain many large pores with an irregular shape and a porous structure due to the three-dimensional structures [45]. The study revealed the presence of several small spherical and clustered structures that enhance the hydrogels' surface area, a crucial factor in boosting their adsorption capacity [46].

BET analysis is employed to ascertain the surface area and particle size by utilizing adsorption and desorption procedures. The BJH analysis is a technique used to study the pore structure of materials, which helps fully understand the properties and potential applications of porous substances [47]. is enclosed in square brackets. The BET and BJH analysis results on the produced hydrogels N3 and N4 are presented in Figures S3 and Table 1.

The results indicate that the N3 gel copolymer exhibits a greater total specific surface area and pore size than the N4 gel copolymer. Table 1 displays the Specific surface area values of 66.9 m^2/g for N3 and 29 m^2/g for N4. The hydrogel N4 can be categorized as mesoporous due to its pore diameter, which has an average value of 29 nm. On the other hand, the hydrogel N3 is classified as macroporous, having an average pore size of 66.9 nm [48]. The results indicate that the prepared hydrogels possess a strong capacity for adsorbing various adsorbents. Clearly, two separate groups of energy sites are accessible for varying pore diameters. Nevertheless, the disparity in their energy levels is negligible. As the probability value of the energy site grows, the adsorption uptake gradually increases due to the presence of high energy level adsorption sites [49].

The thermal properties of all the hydrogel samples were determined using TGA and DSC techniques. Less than 10 mg of each hydrogel sample was taken and subjected to a temperature range of 20-600 °C under N2 gas.

The TGA thermograms were used to calculate several thermal parameters for N3 and N4 hydrogels, including the initial (T_i) and final (T_f) decomposition temperatures, the decomposition temperature at 50% weight loss ($T_{50\%}$), and the char content at 600 ˚C. The DSC thermograms were also used to determine the glass transition temperature (Tg). Figure S4, and Table S2 display all thermal parameters.

At temperatures ranging from 100 to 150 °C, the weight of the prepared hydrogel polymers decreases initially due to the evaporation of a tiny quantity of water. This happens because the hydrophilic groups present are highly attracted to water and are not easily removed, even via drying. This is not considered a decomposition process. The first and second stages of decomposition occur due to the hydrogel chain breaking down at elevated temperatures.

All the prepared hydrogels were used to evaluate the adsorption capacity to remove CR dye. The two best formulations, N3 and N4 gels, had the highest adsorption efficiency for CR dye removal compared to other hydrogels. Therefore, they were chosen to evaluate other factors affecting the adsorption process.

Table 1. BET results for N3 and N4 hydrogels.

Hydrogel	Specific surface area (m^2/g)	Mean pore diameter (nm)
N3	66.9	64.05
N4	29	24.591

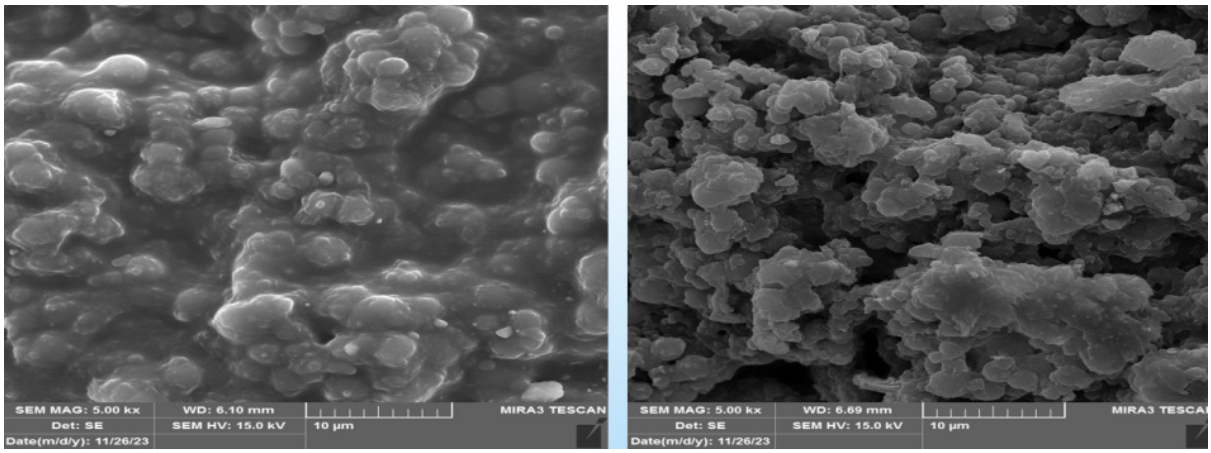

Figure 1. The scanning electron microscope of the swelling state of N1 and N6.

The optimal initial concentration of CR dye, 700 mg L^{-1}, was determined for both chosen adsorbate hydrogels, which give adsorption capacities of about 76.8 % and 72.2% for N3 and N4, respectively.

The pH value significantly impacts the adsorption capacity by increasing or decreasing the interactions between the dye molecules and the surfaces of the adsorbed polymers; this depends on the structure of the dye and the adsorbents [50].

The highest adsorption capacity was achieved in both natural and acidic environments, as depicted in Figure 2. However, the dye was not adsorbed in an acidic environment with a pH of 3 to 5. Instead, the dye underwent a structural change, separating from its water-based solution. It provided a distinct wavelength completely dissimilar to the documented wavelength of the CR dye reported in the literature.

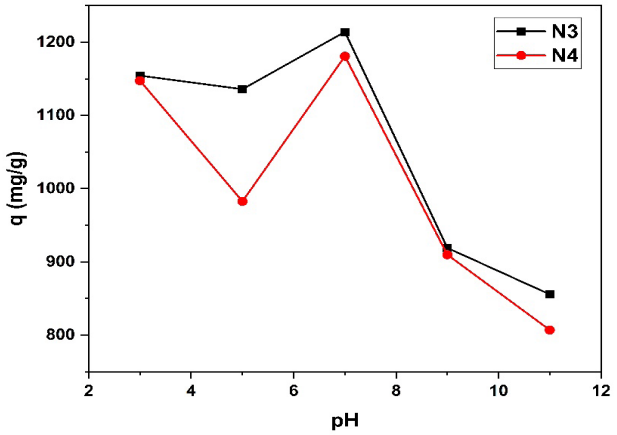

Figure 2. The effect of pH on the adsorption of CR dye on prepared N3 and N4.

The adsorption capacity decreases as the pH value rises to the alkaline level because of the augmentation in hydroxyl ions and ionization of the negative active groups on the polymeric adsorbents. This results in repulsion between the functional groups of the adsorbent and the negatively charged dye molecule. Based on Figure 2, it is evident that the pH with the highest adsorption performance was at a value of seven. Therefore, this particular pH was selected for further investigation in the following adsorption studies.

The contact time between the adsorbent and the adsorbate is essential to the adsorption process. It is helpful to estimate the required time to reach the equilibrium state [51]. The contact time was determined at the optimal pH and concentration of CR dye at three different temperatures (35, 45, 65) °C for adsorbents N3 and N4, as depicted in Figure 3. Both adsorbates N3 and N4 exhibited an initial rapid increase in adsorption, followed by a gradual increase until reaching equilibrium after 150 minutes.

At 35°C, both N3 and N4 showed an adsorption capacity of 1216 and 1171, respectively. The adsorption percentage was 86.9 % and 83.6 % for N3 and N4, respectively. At 45°C, equilibrium was reached in 120 and 150 minutes, with an adsorption capacity increase to 1303 and 1260, and the percentage of adsorption increased to 93.1% and 90.0% for N3 and N4, respectively. At a temperature of 65°C, the adsorption capacity for both N3 and N4 increased continuously to 1365 and 1328, respectively. The adsorption percentage also increased to 97.5% and 94.9%, respectively. However, the equilibrium time decreased to 90 minutes for N3 and 120 minutes for N4.

The results clearly demonstrate that higher temperatures reduce the contact time between the dyes and the adsorbent surfaces. Nevertheless, the increased kinetic energy increases both the ability to attract and retain molecules and the proportion of molecules attracted. With increasing temperatures, more molecules acquire the necessary energy for adsorption [52].

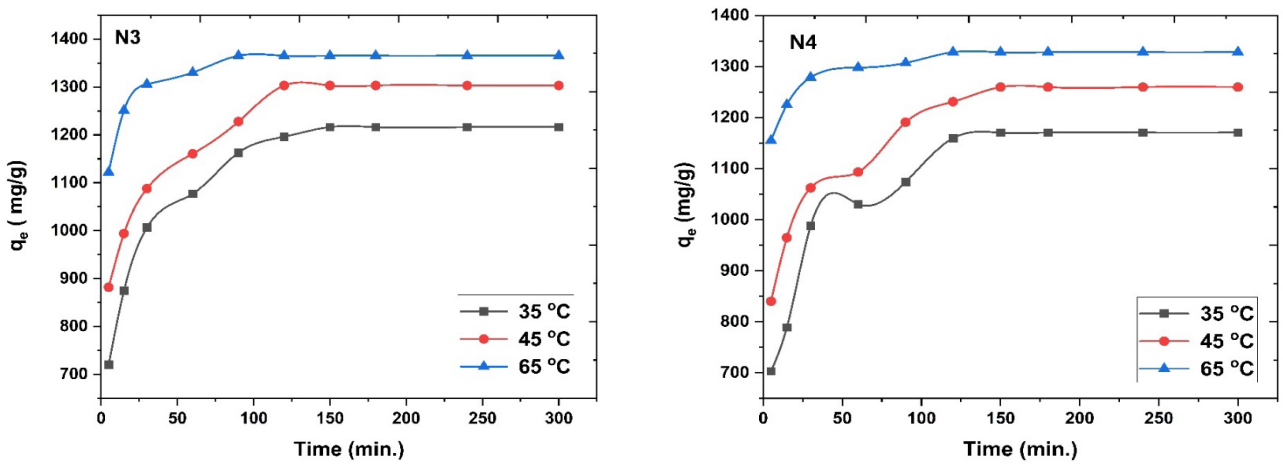

Figure 3. The effect of Temp. on the equilibrium time and the adsorption capacity of CR dye on prepared N3 and N4 at 35°C.

The isotherms study (Langmuir and Freundlich) for surfaces N3 and N4 showed that both followed the Langmuir isotherm; this was inferred from the Correlation factor R^2, as it found that the Langmuir isotherm had a higher R^2 value of (0.9998-0.999), compared to the Freundlich isotherm which had an R^2 value of 0.933-0.9362. Additionally, the Langmuir separation factor RL value was (0.002849, 0.003381), which indicates that the adsorption system is favorable, and the smaller value refers to higher attraction to the CR dye [53], as in Figures S5 and S6.

Adsorption kinetics is an essential factor to consider when designing an adsorption system. It controls the adsorption rate and the equilibrium time [54]. It provides important information about the adsorption process, such as the adsorption constant K, the Correlation coefficient R^2, and the theoretical (the expected) adsorption capacity (q exp). This is illustrated in Figures S7, S8 and S9 and Tables S3, S4, and S5 regarding the Pseudo (first and second) order and inter particles diffusion kinetics, respectively.

By comparing R^2 values for Kinetics models of (first, second) order and interparticle models and comparing the experimental and theoretical adsorption capacity, it can be observed from Table S3 that the experimental adsorption capacity (q exp) is significantly different from the theoretical capacity (q theo), indicating that the first-order model does not apply to the adsorption system. However, Table S4 shows that the two values are very close, suggesting that the second-order model is the most probable for both adsorbents N3 and N4, meaning that chemical adsorption is the rate-determining step.

For the interparticle models, c refers to the thickness of the boundary layer of adsorption, which increases with temperature. Kp also increases with temperature, indicating that temperature enhances the interparticle dispersion of molecules. In Figure S8, it is evident that the linear relationship does not pass through the origin, indicating that there is no intersection to become zero. This means that diffusion is not a comprehensive step that controls the adsorption process.

The thermodynamic parameters play an important role in predicting adsorption behaviour and depend significantly on the temperature; Figure S10 and Table S6 indicate the values of thermodynamic constants and variables.

A positive value of ΔH indicates that the adsorption process was endothermic. On the other hand, a positive value of ΔS means that there was a lot of randomness, which made the surfaces and dye molecules closer together. This means that the molecules have a high level of freedom, which allows them to have a good approach with the adsorbents. The negative values of ΔG show that the adsorption process happened spontaneously and increased with increasing temperature, meaning that the adsorption of the CR dye was favoured dynamically by increasing the temperature [56].

The activation energy indicates the adsorption type, whether physical or chemical. When the activation energy is low, less than 40 KJ/mole, it indicates physical adsorption, while the activation energy higher than 40 KJ/mole indicates chemical adsorption. According to Table S6 and Figure S11, the adsorption of CR dye on N3 and N4 shows that chemical adsorption is the main type of adsorption for N3, while physical adsorption is the main type of adsorption for N4.

Desorption studies are essential to understanding the adsorption mechanism [57]. Therefore, we employed adsorption-desorption processes, and Figure 4 presents the results. The results showed that CR desorption from N3 and N4 adsorbents was weak to moderate. Sodium hydroxide solution was the best eluent for CR desorption from N3 and N4 adsorbents. The CR desorption from N4 gave higher values than N3, which was compatible with its lower activation energy.

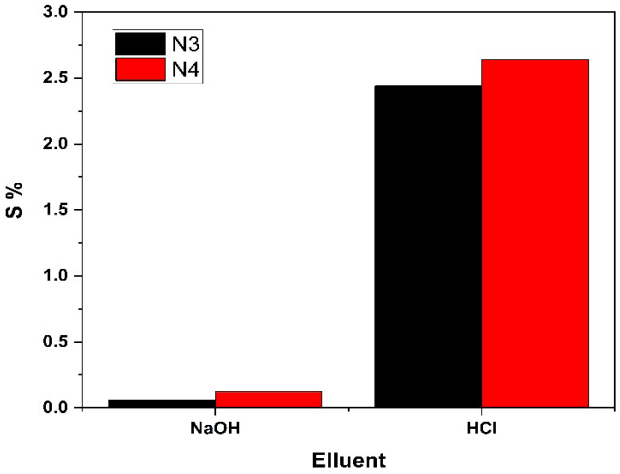

Figure 4. Desorption of CR dye with different eluents.

Conclusion

The study showed that the prepared hydrogel surfaces are effective adsorbents for anionic dyes like Congo Red (CR). The results show that both pH and temperature influence the adsorption rate. As the adsorption rate increased with temperature, the best adsorption was at (65° C) and in pH 7. The Langmuir model predicted pseudo-second-order kinetics for CR dye adsorption on hydrogels. The process involved chemisorption, endothermic reactions, randomness, and spontaneous adsorption, with NaOH proving the most effective eluent for CR dye desorption.

References

1. Singh, N., Poonia, T., Siwal, S. S., Srivastav, A. L., Sharma, H. K., & Mittal, S. K. (2022). Challenges of water contamination in urban areas. In *Current directions in water scarcity research* (Vol. 6, pp. 173-202). Elsevier.

2. Mohammad, R. E. A., Birniwa, A. H., Abdullahi, S. S. A., & Jagaba, A. H. (2023). Decolourization of textile dyes using CNT-based hybrid materials. In

Nanohybrid Materials for Treatment of Textiles Dyes (pp. 119-156). Singapore: Springer Nature Singapore.

3. Toledo, P. V., Bernardinelli, O. D., Sabadini, E., & Petri, D. F. (2020). The states of water in tryptophan grafted hydroxypropyl methylcellulose hydrogels and their effect on the adsorption of methylene blue and rhodamine B. *Carbohydrate Polymers*, *248*, 116765.

4. Esmaeili, A. (2023). Textile Dyes Removal Using Silica-Dendrimer Hybrid Materials. In *Nanohybrid Materials for Treatment of Textiles Dyes* (pp. 303-342). Singapore: Springer Nature Singapore.

5. Islam, T., Repon, M. R., Islam, T., Sarwar, Z., & Rahman, M. M. (2023). Impact of textile dyes on health and ecosystem: A review of the structure, causes, and potential solutions. *Environmental Science and Pollution Research*, *30*(4), 9207-9242.

6. Benkhaya, S., M'rabet, S., & El Harfi, A. (2020). A review of classifications, recent synthesis and applications of textile dyes. *Inorganic Chemistry Communications*, *115*, 107891.

7. Kavitha, G., Vinoth Kumar, J., Arulmozhi, R., Kamath, S. M., Priya, A. K., Rao, K. S., & Abirami, N. (2022). 2D graphene supported nickel oxide nano-composite for fiber optic ethanol gas sensing, removal of azo dye, and biological activity. *Journal of Materials Science: Materials in Electronics*, 1-14.

8. Radoor, S., Karayil, J., Jayakumar, A., Kandel, D. R., Kim, J. T., Siengchin, S., & Lee, J. (2023). Recent advances in cellulose-and alginate-based hydrogels for water and wastewater treatment: A review. *Carbohydrate Polymers*, 121339.

9. Bustos-Terrones, Y. A., Hermosillo-Nevárez, J. J., Ramírez-Pereda, B., Vaca, M., Rangel-Peraza, J. G., Bustos-Terrones, V., & Rojas-Valencia, M. N. (2021). Removal of BB9 textile dye by biological, physical, chemical, and electrochemical treatments. *Journal of the Taiwan Institute of Chemical Engineers*, *121*, 29-37.

10. Siddiqui, S. I., Allehyani, E. S., Al-Harbi, S. A., Hasan, Z., Abomuti, M. A., Rajor, H. K., & Oh, S. (2023). Investigation of Congo Red Toxicity towards Different Living Organisms: A Review. *Processes*, *11*(3), 807.

11. Arab, C., El Kurdi, R., & Patra, D. (2022). Effect of pH on the removal of anionic and cationic dyes using zinc curcumin oxide nanoparticles as adsorbent. *Materials Chemistry and Physics*, *277*, 125504.

12. Zhu, H., Chen, S., Duan, H., He, J., & Luo, Y. (2023). Removal of anionic and cationic dyes using porous chitosan/carboxymethyl cellulose-PEG hydrogels: Optimization, adsorption kinetics, isotherm and thermodynamics studies. *International Journal of Biological Macromolecules*, *231*, 123213.

13. Villabona-Ortíz, Á., Figueroa-Lopez, K. J., & Ortega-Toro, R. (2022). Kinetics and adsorption equilibrium in the removal of azo-anionic dyes by modified cellulose. *Sustainability*, *14*(6), 3640.

14. Nguyen, H. T., Ngwabebhoh, F. A., Saha, N., Saha, T., & Saha, P. (2022). Gellan gum/bacterial cellulose hydrogel crosslinked with citric acid as an eco-friendly green adsorbent for safranin and crystal violet dye removal. *International Journal of Biological Macromolecules*, *222*, 77-89.

15. Qu, J., Meng, Q., Peng, W., Shi, J., Dong, Z., Li, Z., ... & Zhang, Y. (2023). Application of functionalized biochar for adsorption of organic pollutants from environmental media: Synthesis strategies, removal mechanisms and outlook. *Journal of Cleaner Production*, 138690.

16. Luo, R., Wang, X., Huang, T., & Tu, C. (2023). Investigation on the methods of measuring aggregate surface energy based on spreading pressure. *Construction and Building Materials*, *378*, 131135.

17. Liu, X., Tournassat, C., Grangeon, S., Kalinichev, A. G., Takahashi, Y., & Marques Fernandes, M. (2022). Molecular-level understanding of metal ion retention in clay-rich materials. *Nature Reviews Earth & Environment*, *3*(7), 461-476.

18. Aragaw, T. A., & Alene, A. N. (2022). A comparative study of acidic, basic, and reactive dyes adsorption from aqueous solution onto kaolin adsorbent: Effect of operating parameters, isotherms, kinetics, and thermodynamics. *Emerging Contaminants*, *8*, 59-74.

19. Umeh, A. C., Hassan, M., Egbuatu, M., Zeng, Z., Al Amin, M., Samarasinghe, C., & Naidu, R. (2023). Multicomponent PFAS sorption and desorption in common commercial adsorbents: Kinetics, isotherm, adsorbent dose, pH, and index ion and ionic strength effects. *Science of The Total Environment*, *904*, 166568.

20. Hu, Y. Y., Pan, C., Liu, S., Wang, X., Zheng, X., Hu, F., ... & Peng, X. (2022). Ultra-fast adsorption of radioactive-U (VI) and Cs (I) with high adsorption capacity towards CAA@ MgAlFe spongy-like aerogel: mechanism and application feasibility study. *Journal of Nuclear Materials*, *559*, 153463.

21. Pan, L., Wang, C., Wu, W., Li, X., Ma, S., Li, C., ... & Ou, J. (2022). Bioinspired honeycomb-like 3D architectures self-assembled from chitosan as dual-functional membrane for effective adsorption and detection of copper ion. *Microporous and Mesoporous Materials*, *335*, 111859.

22. Ahmadian, M., & Jaymand, M. (2023). Interpenetrating polymer network hydrogels for removal of synthetic dyes: A comprehensive review. *Coordination Chemistry Reviews*, *486*, 215152.

23. Yang, Y., Zhu, Q., Peng, X., Sun, J., Li, C., Zhang, X., ... & Zhang, Y. (2022). Hydrogels for the removal of the methylene blue dye from wastewater: A review. *Environmental Chemistry Letters*, *20*(4), 2665-2685.

24. Safarzadeh, H., Peighambardoust, S. J., Mousavi, S. H., Foroutan, R., Mohammadi, R., & Peighambardoust, S. H. (2022). Adsorption ability evaluation of the poly (methacrylic acid-co-acrylamide)/cloisite 30B nanocomposite hydrogel as a new adsorbent for cationic dye removal. *Environmental Re-*

search, *212*, 113349.

25. Blažic, R., Marušić, K., & Vidović, E. (2023). Swelling and Viscoelastic Properties of Cellulose-Based Hydrogels Prepared by Free Radical Polymerization of Dimethylaminoethyl Methacrylate in Cellulose Solution. *Gels*, *9*(2), 94.

26. Sood, A., Dev, A., Das, S. S., Kim, H. J., Kumar, A., Thakur, V. K., & Han, S. S. (2023). Curcumin-loaded alginate hydrogels for cancer therapy and wound healing applications: A review. *International Journal of Biological Macromolecules*, 123283.

27. Frent, O. D., Vicas, L. G., Duteanu, N., Morgovan, C. M., Jurca, T., Pallag, A., ... & Marian, E. (2022). Sodium alginate—Natural microencapsulation material of polymeric microparticles. *International Journal of Molecular Sciences*, *23*(20), 12108.

28. Wan, P., Wu, S., Liu, Q., Zou, Y., Zhao, Z., & Chen, S. (2022). Recent advances in calcium alginate hydrogels encapsulating rejuvenator for asphalt self-healing. *Journal of Road Engineering*.

29. Halbus, A. F., Salman, J. M., Lafta, A. J., Athab, Z. H., Hasan, F. M., Kamil, A. M., & Hussein, F. H. (2017). Equilibrium, isotherms and thermodynamic studies of congo red adsorption onto Ceratophyllum Demersum.

30. Abd-Alwahab, D. R., Abbas, S. H., & Haddad, A. M. (2022). Removal of Congo red by copoly (DMAE-MA-AMPS) hydrogels for water treatment. *Journal of Kufa for Chemical Sciences*, *2*(9), 409-435.

31. Alwattar, A. A., Haddad, A., Moore, J., Alshareef, M., Bartlam, C., Woodward, A. W., ... & Quayle, P. (2021). Heavy metal sensors and sequestrating agents based on polyaromatic copolymers and hydrogels. *Polymer International*, *70*(1), 59-72.

32. Zhang, Y., He, Q., Kobayashi, K., Kusumi, R., & Wada, M. (2023). Hydrogels from dextran/carboxymethyl cellulose exhibited high post-drying swelling ratios and recovery. *Cellulose*, *30*(1), 263-276.

33. Alharbi, R. A., Alminderej, F. M., Al-Harby, N. F., Elmehbad, N. Y., & Mohamed, N. A. (2023). Preparation and characterization of a new bis-uracil chitosan-based hydrogel as efficient adsorbent for removal of anionic Congo red dye. *Polymers*, *15*(6), 1529.

34. Webber, J. J., Etzold, M. A., & Worster, M. G. (2023). A linear-elastic–nonlinear-swelling theory for hydrogels. Part 2. Displacement formulation. *Journal of Fluid Mechanics*, *960*, A38.

35. Vairavel, P., Rampal, N., & Jeppu, G. (2023). Adsorption of toxic Congo red dye from aqueous solution using untreated coffee husks: Kinetics, equilibrium, thermodynamics and desorption study. *International Journal of Environmental Analytical Chemistry*, *103*(12), 2789-2808.

36. Ghosh, N., Sen, S., Biswas, G., Saxena, A., & Haldar, P. K. (2023). Adsorption and desorption study of reusable magnetic iron oxide nanoparticles modified with Justicia adhatoda leaf extract for the removal of textile dye and antibiotic. *Water, Air, & Soil Pollution*, *234*(3), 202.

37. Su, Z. B.; Hu, S. R.; Weng, W.; Li, S. X.; Guo, H. X.; Wu, W. B., NH2-rich polymer/graphene oxide use as a novel adsorbent for removal of Cu (II) from aqueous solution. Chemical Engineering Journal, 263, 280-289 (2015).

38. Mizhir, A., Abdulwahid, A., & Al-Lami, H. (2020). Chemical functionalization graphene oxide for the adsorption behavior of bismarck brown dye from aqueous solutions. *Egyptian Journal of Chemistry*, *63*(5), 1679-1696.

39. Ahmad, N., Bano, D., Jabeen, S., Ahmad, N., Iqbal, A., Anwer, A. H., & Jeong, C. (2023). Insight into the adsorption thermodynamics, kinetics, and photocatalytic studies of polyaniline/SnS2 nanocomposite for dye removal. *Journal of Hazardous Materials Advances*, *10*, 100321.

40. Takahashi, I., & Allonas, X. (2023). Novel Peroxide-Free redox initiator based on Saccharin/Electron Donor/Copper salt for radical polymerization. *European Polymer Journal*, *188*, 111900.

41. Shahruzzaman, M., Islam, M. M., Islam, M. S., Sakib, M. N., Mallik, A. K., Haque, P., & Rahman, M. M. (2020). Semi-IPN Systems for Drug Delivery. *Interpenetrating Polymer Network: Biomedical Applications*, 205-236.

42. Berradi, A., Aziz, F., Achaby, M. E., Ouazzani, N., & Mandi, L. (2023). A Comprehensive Review of Polysaccharide-Based Hydrogels as Promising Biomaterials. *Polymers*, *15*(13), 2908.

43. Zhan, Z., Chen, L., Wang, C., Shuai, Y., Duan, H., & Wang, Z. (2023). Super Water-Storage Self-Adhesive Gel for Solar Vapor Generation and Collection. *ACS Applied Materials & Interfaces*, *15*(6), 8181-8189.

44. Martinez-Garcia, F. D., Fischer, T., Hayn, A., Mierke, C. T., Burgess, J. K., & Harmsen, M. C. (2022). A beginner's guide to the characterization of hydrogel microarchitecture for cellular applications. *Gels*, *8*(9), 535.

45. Wu, Z., Zhang, P., Zhang, H., Li, X., He, Y., Qin, P. & Yang, C., "Tough porous nanocomposite hydrogel for water treatment", J. Hazard. Mater, 421(1), 126-754 (2022).

46. Lei, C., Bian, Y., Zhi, F., Hou, X., Lv, C., & Hu, Q. (2022). Enhanced adsorption capacity of cellulose hydrogel based on corn stalk for pollutants removal and mechanism exploration. *Journal of Cleaner Production*, *375*, 134130.

47. Irwansyah, F. S.; Amal, A. I.; Diyanthi, E. W.; Hadisantoso, E. P.; Noviyanti, A. R.; Eddy, D. R.; Risdiana, R. How to read and determine the specific surface area of inorganic materials using the Brunauer-Emmett-Teller (BET) method. AJSE. 2024, 4, 1, 61-70. DOI: https://doi.org/10.17509/ajse.v4i1.60748.

48. Miao, Y.; Zhai, S.; Pan, M.; Sun, E.; Xia, C.; Lyu, J.; Imai, T. New insight into cell wall pore structure in brown-rotted wood and its utilization as a new low-cost, sustainable adsorbent. Ind. Crops Prod. 2024, 208, 117843. DOI:10.1016/j.indcrop.2023.117843.

49. Lee, S. J.; Yu, Y.; Jung, H. J.; Naik, S. S.;

Yeon, S.; Choi, M. Y. Efficient recovery of palladium nanoparticles from industrial wastewater and their catalytic activity toward reduction of 4-nitrophenol. Chemosphere. 2021, 262, 128358. DOI: 10.1016/j.chemosphere.2020.128358.

50. Qiu, B., Shao, Q., Shi, J., Yang, C., & Chu, H. (2022). Application of biochar for the adsorption of organic pollutants from wastewater: Modification strategies, mechanisms and challenges. *Separation and Purification Technology*, 121925.

51. Zahid, M. et al., "Hybrid nanomaterials for water purification", Multifunct. Hybrid Nanomater. Sustain. Agri-Food Ecosyst, 155– 188 (2020).

52. Shahinpour, A., Tanhaei, B., Ayati, A., Beiki, H., & Sillanpää, M. (2022). Binary dyes adsorption onto novel designed magnetic clay-biopolymer hydrogel involves characterization and adsorption performance: Kinetic, equilibrium, thermodynamic, and adsorption mechanism. *Journal of Molecular Liquids*, *366*, 120303.

53. Khader, E. H., Khudhur, R. H., Abbood, N. S., & Albayati, T. M. (2023). Decolourisation of anionic azo dye in industrial wastewater using adsorption process: Investigating operating parameters. *Environmental Processes*, *10*(2), 34.

54. Aniagor, C. O., Igwegbe, C. A., Ighalo, J. O., & Oba, S. N. (2021). Adsorption of doxycycline from aqueous media: a review. *Journal of Molecular Liquids*, *334*, 116124.

55. Bakr, A. A., Sayed, N. A., Salama, T. M., Ali, I. O., Gayed, R. A., & Negm, N. A. (2018). Kinetics and thermodynamics of Mn (II) removal from aqueous solutions onto Mg-Zn-Al LDH/montmorillonite nanocomposite. *Egyptian journal of petroleum*, *27*(4), 1215-1220.

56. Alghamdi, A. A., Al-Odayni, A. B., Abduh, N. A., Alramadhan, S. A., Aljboar, M. T., & Saeed, W. S. (2021). Adsorptive performance of polypyrrole-based KOH-activated carbon for the cationic dye crystal violet: kinetic and equilibrium studies. *Adsorption Science & Technology*, *2021*, 1-11.

57. Soldatkina, L. & Zavrichko, M., "Equilibrium, kinetic, and thermodynamic studies of anionic dyes adsorption on corn stalks modified by cetylpyridinium bromide", *Colloids and Interfaces*, 3(1), 1-16 (2019).